

Radiative improvement of the lattice NRQCD action using the background field method with applications to quarkonium spectroscopy

T.C. Hammant,¹ A.G. Hart,^{2,3} G.M. von Hippel,⁴ R.R. Horgan,¹ and C.J. Monahan¹

¹*Department of Applied Mathematics and Theoretical Physics, University of Cambridge, Centre for Mathematical Sciences, Cambridge CB3 0WA, United Kingdom*

²*Cray Exascale Computing Research Initiative, University of Edinburgh,*

King's Buildings, Mayfield Road, Edinburgh EH9 3JZ, United Kingdom

³*SUPA, School of Physics and Astronomy, University of Edinburgh,*

King's Buildings, Mayfield Road, Edinburgh EH9 3JZ, United Kingdom

⁴*Institut für Kernphysik, University of Mainz, Becher-Weg 45, 55099 Mainz, Germany*

We apply the background field (BF) method to Non-Relativistic QCD (NRQCD) on the lattice in order to determine the one-loop radiative corrections to the coefficients of the NRQCD action in a manifestly gauge-covariant manner by matching the NRQCD prediction for particular on-shell processes with those of relativistic continuum QCD. We explain how the BF method is implemented in automated perturbation theory and discuss the technique for matching the relativistic and non-relativistic theories. We compute the one-loop radiative corrections to the $\sigma \cdot \mathbf{B}$ and Darwin terms for the NRQCD action currently used in simulations, as well as the one-loop coefficients of the spin-dependent $O(\alpha^2)$ four-fermion contact terms. The effect of the corrections on the hyperfine splitting of bottomonium is estimated using earlier simulation results [1]; the corrected lattice prediction is found to be in agreement with experiment. Agreement of the hyperfine splitting of bottomonium and the B -meson system is confirmed by recent simulation studies [2, 3] which include our NRQCD radiative corrections for the first time.

PACS numbers: 12.38.Bx, 12.38.Gc

I. INTRODUCTION

The decays of hadrons containing bottom quarks provide some of the most stringent tests of the Standard Model (SM) so far, but direct simulations of the bottom quark in lattice QCD remain fraught with problems due to discretization effects arising from the large mass of the bottom quark in conjunction with current limitations on achievable lattice spacings. An alternative is provided by Non-Relativistic QCD (NRQCD) [4], an effective field theory for heavy quarks whose use in describing heavy-flavour hadrons has so far met with considerable success [1] and which represents one important approach to obtaining accurate predictions for flavour physics observables and testing the limits of the SM. However, until recently the NRQCD actions used in lattice simulations did not include radiative corrections to the action, limiting the accuracy to which such important quantities as the $\Upsilon\text{-}\eta_b$ hyperfine splitting could be predicted [5]. This is in stark contrast to the situation of Non-Relativistic QED (NRQED), for which the radiative improvements to the action have long been known, leading to highly precise theoretical predictions for muonium hyperfine structure and for positronium decay [6–8]. Achieving similar precision for NRQCD predictions by including the radiative improvements in the NRQCD action is therefore highly desirable. However, a crucial difference to the NRQED case is that the strongly interacting non-abelian nature of QCD and NRQCD imposes confinement and calls for a lattice implementation of NRQCD; this means that the complete $1/(Ma)^n$ structure of all quantities must be retained, as opposed to the situation in (con-

tinuum) NRQED, where there are ways to drop terms in $(\Lambda/M)^n$ consistently. A further complication arises from infrared (IR) divergences, which turn out to play a significant rôle in the non-abelian case.

In this paper, we follow up on our letter [9] where we presented the first calculation of radiative corrections to the lattice NRQCD action using the background field (BF) method. We proceed by computing the effective action in both continuum QCD and lattice NRQCD at one loop and matching the latter term by term to the non-relativistic reduction of the former. In particular, we determine the $O(\alpha_s)$ correction to the coefficient c_4 of the chromomagnetic $\sigma \cdot \mathbf{B}$ operator and the leading contributions to the coefficients of the spin-dependent four-fermion contact operators in the NRQCD action, as required in order to enable a more precise determination of the hyperfine structure of heavy quarkonia in NRQCD. Using our results, we are able to estimate the $O(\alpha_s^2)$ correction to the hyperfine splitting of the S-wave bottomonium states using simulation data from [1], giving a corrected value of 72(3)(5)(3) MeV, which agrees with the experimental value of 69.3(2.8) MeV [10]. The correction has the additional beneficial effect of reducing the lattice spacing dependence, placing the remaining $O(\alpha^2)$ discretization errors well below other sources of error.

We remark that our calculation reported here completes the one-loop radiative improvement of quark bilinear terms to $O(v^4)$ in the NRQCD action for which the improvement of the purely kinetic terms was reported in [2]: see section III.

In section II we discuss in some more detail the ap-

proach to matching using the BF method and discuss the gauge invariance of our results; in sections IV and V, we proceed to apply the BF method to the matching of the chromomagnetic and Darwin terms in the NRQCD action. The four-fermion interactions in NRQCD are the topic of section VI, where we derive results for the spin-dependent four-fermion operators and explain the difficulties in matching their spin-independent counterparts, which will be the topic of a future paper. We apply our results to the hyperfine splitting and S-wave mass shifts in section VII before summarizing our results in section VIII.

In the following we denote the perturbative expansion for a generic quantity w as $w = \sum_{n=0} w^{(n)} \alpha_s^n$. Where $w^{(n)}$ contains IR divergences, the IR finite part is denoted with a tilde: $\tilde{w}^{(n)}$.

II. THE BACKGROUND FIELD METHOD FOR LATTICE NRQCD

The BF method [11–15] is well established as a tool to compute the effective action in quantum field theory, which has a number of very attractive features: firstly, QCD in background field gauge (BFG) satisfies a set of abelian-like Ward identities reducing the number of calculations needed in order to renormalize it. Secondly, the existence of a residual gauge invariance in BFG implies that only gauge-covariant operators can appear in the effective action, which is of particular importance when considering operators of dimension $D > 4$ as required in an effective theory, where a loss of gauge-covariance would herald a proliferation of additional operators.

A method to derive a unique effective action is given by the Vilkovisky-DeWitt (VDW) technique and one choice is to use the Landau-DeWitt gauge corresponding to the BF generalization of Landau gauge [16]. Whether or not this approach is applicable to our matching procedure remains to be investigated. However, for our purposes, the VDW method is not necessary since we are able to perform our matching solely using on-shell quantities including S-matrix elements which can be given an unambiguous physical interpretation.

The BF method is indispensable to our matching procedure. As an effective theory, NRQCD has operators of dimension $D > 4$ appearing in the action, and BFG is needed to ensure a gauge-covariant form of the effective action; this is not guaranteed nor likely without using the BF formalism. It should be noted that the appearance of gauge-non-covariant $D > 4$ operators in the effective action would not in and of itself be incorrect; however, by obscuring the gauge symmetry of the theory, they would hinder a physical interpretation of the results and significantly complicate the calculations. Moreover, without the use of BFG, a further source of complexity would arise from the appearance of ultraviolet (UV) logarithms in the coefficients of operators in the effective action, whose contributions to physical processes would

have to cancel against the contributions from the additional non-gauge-covariant operators.

Finally, the BF method makes our work easier and tractable because the QED-like Ward identities in BFG are enough to render the one-particle irreducible (1PI) vertex function finite, so that only the gluonic self-energy renormalizes the coupling, whereas the BF itself is not renormalized. Since these statements hold in both QCD and NRQCD, we are able to match the two theories by equating two quantities that are UV finite and thus we can use different regulators on either side. In particular, the QCD vertex can be calculated analytically in the continuum using dimensional regularization (DR), or numerically on fine lattices approaching the continuum limit, where the latter is particularly convenient for checking the gauge-parameter independence of the result since analytical calculations for arbitrary values of the gauge parameter tend to become rather involved.

The remaining issue is how to regularize the infrared (IR) divergences which arise at intermediate steps in our calculation. The radiative corrections to the coefficients in the NRQCD action are, and must be, IR finite: they cannot depend on any scheme to regularize IR divergences. Two kinds of IR divergences arise. The first are those that occur in the continuum calculation of the diagrams. These divergences are a-priori independent of the non-zero lattice spacing a and must match directly between the relativistic QCD and NRQCD calculations. The second are lattice artifact IR divergences that occur solely in the NRQCD one-loop calculations, and the contributions from the set of diagrams under consideration must cancel consistently within the NRQCD calculation since they depend on a . That the IR divergences match or cancel in this way is a strong consistency check on our calculations. In NRQCD we are also able to calculate both kinds of IR divergence analytically in every case considered and also numerically and agreement between the two approaches is a further check on our results.

Whilst it might, in principle, be possible to eliminate the continuum IR divergences by subtracting the integrand in continuum QCD from the equivalent one in NRQCD, this approach is numerically very difficult. It is compounded by the need to also eliminate the lattice artifact IR divergences in the same way, otherwise the use of an IR regulation scheme is, in any case, inevitable; this would be numerically very hard to accomplish. We cannot use dimensional regularization to regulate the IR divergences since these are not applicable for lattice field theories. There are a number of other methods that can be used in our case.

Twisted boundary conditions (TWB) can be applied corresponding to matching the non-abelian gauge theories in a region of finite extent L in two or three spatial dimensions [17–19]. The TWB eliminate the zero modes for the non-abelian gauge field and give a gauge invariant regulation of IR divergences with a mass-scale $2\pi/3L$ for the $SU(3)$ gauge theory. Although there are extra complications in the background field approach, TWB

are relatively straightforward to implement for numerical lattice calculations and have been used to carry out improvement calculations [19, 20]. However, they are difficult to implement analytically for the continuum QCD calculations and although there is progress in this area we choose not to implement the TWB.

The NRQCD action is a derivative expansion and the strategy is to match the expansion in independent external momenta for each amplitude considered. IR divergences can be regulated by using a small but non-zero momentum transfer, q say, in the diagram concerned. After cancellation of the IR singularities we may safely set $q = 0$. The application of this method to diagrams with more than one loop needs careful thought but is certainly an option for one-loop calculations.

We regulate the IR divergences in both QCD and NRQCD using a gluon mass μ . This is known to be correct for diagrams which have a QED-like topology: in QCD the difference is a simple overall colour factor. In general, a non-zero gluon mass in QCD breaks gauge invariance and in our calculation the one-loop diagrams for matching the quark bi-linear operators, which give the chromodynamic form factors, contain three-gluon vertices and the use of a gluon mass IR regulator needs justification. We note that at one-loop the diagrams are identical to those that would arise in the Curci-Ferrari theory [21, 22] which is renormalizable and known to recover QCD in the $\mu \rightarrow 0$ for gauge-invariant quantities; the introduction of a non-zero gluon mass by extending QCD to the Curci-Ferrari formulation is a mechanism for regulating IR divergences [21–29]. We match on-shell gauge-invariant physical processes and in our final result all IR divergences cancel to give IR-finite gauge-covariant counterterms in NRQCD and the limit $\mu \rightarrow 0$ can be taken. Diagrams with more than one loop in Curci-Ferrari theory will contain extra contributions compared with the same process in QCD. The Curci-Ferrari theory on a lattice is formulated and discussed by von Smekal et al. [30].

For the case of matching the quark bi-linear operators another approach is to introduce gluon masses

by the spontaneous symmetry breaking of $SU(3) \rightarrow U(1)_3 \times U(1)_8$ [31] and calculate in the renormalizable R_ξ gauge. The unbroken abelian gauge groups are generated, respectively, by the T_3 and T_8 $SU(3)$ generators. In general, QCD is not recovered in the zero mass limit since there remain massless scalar fields. However, the one-loop diagrams that we calculate are identical in both QCD and the spontaneously broken theory. In this case, our present calculation corresponds to computing the quark bi-linear form factors for the $U(1)_8$ (massless) gluon.

An alternative justification was established by Kautsky [32]. In BFG the Ward Identities in QCD give a QED-like relationship between the quark wavefunction renormalization constant, Z_2 , and the vertex renormalization constant, Z_1 , namely $Z_1 = Z_2$; a violation of this equality would signal a breakdown of gauge invariance. Kautsky showed in BFG that at one loop this equality does hold when the IR divergences in the diagrams concerned are regulated by a non-zero gluon mass. This is a crucial test of this approach for regulating IR divergences.

An important observation, that we verify, is that the results of calculating the physical process used for the matching procedure in NRQCD and QCD are separately independent of the gauge parameter multiplying the BF gauge-fixing term in the action: the NRQCD radiative counterterms are both gauge-covariant and independent of the gauge parameter.

III. THE NRQCD ACTION

The lattice NRQCD action up to and including $O(v^6)$ operators is given by [4]

$$S_{NRQCD} = \sum_{x,\tau} \psi^\dagger(x,\tau) [\psi(x,\tau) - K(\tau)\psi(x,\tau-a)] , \quad (1)$$

with the kernel

$$K(\tau) = \left(1 - \frac{a\delta H}{2}\right) \left(1 - \frac{aH_0}{2n}\right)^n U_4^\dagger \left(1 - \frac{aH_0}{2n}\right)^n \left(1 - \frac{a\delta H}{2}\right) , \quad (2)$$

where H_0 is the standard NRQCD kinetic operator, $H_0 = \Delta^{(2)}/2M$.

The quark Green function satisfies the evolution equation

$$G(\mathbf{x}, t+a) = K(t+a)G(\mathbf{x}, t) + \delta_{x,0}\delta_{t+a,0} , \quad (3)$$

where $G(\mathbf{x}, t)$ vanishes for $t < 0$. The kernel K is constructed so as to give an evolution that is symmetric with respect to time reversal, and leads to a smaller wave function renormalization than some other formulations [33].

The parameter n was introduced to prevent instabilities at large momenta due to the kinetic energy operator [34] (it is easy to see that the Green function defined by Eq. (3) diverges if $aH_0/2n > 2$). For a given β and lattice spacing we therefore have a minimum n value. For the values of lattice spacing used by the HPQCD collaboration $n = 2$ or $n = 4$ suffices.

The interaction terms for the “full NRQCD” action are given by,

$$\begin{aligned} \delta H_{full} = & -c_1 \frac{(\Delta^{(2)})^2}{8(Ma)^3} \\ & + c_2 \frac{ig}{8M^2} \left(\mathbf{\Delta}^{(\pm)} \cdot \tilde{\mathbf{E}} - \tilde{\mathbf{E}} \cdot \mathbf{\Delta}^{(\pm)} \right) \\ & - c_4 \frac{g}{2M} \boldsymbol{\sigma} \cdot \tilde{\mathbf{B}} - c_3 \frac{g}{8M^2} \boldsymbol{\sigma} \cdot \left(\tilde{\mathbf{\Delta}}^{(\pm)} \times \tilde{\mathbf{E}} - \tilde{\mathbf{E}} \times \tilde{\mathbf{\Delta}}^{(\pm)} \right) \\ & + c_5 \frac{\Delta^{(4)}}{24M} - c_6 \frac{(\Delta^{(2)})^2}{16nM^2}, \end{aligned} \quad (4)$$

including operators with coefficients c_5 and c_6 to remove the leading discretization artifacts in the improved NRQCD kinetic operator at $O(a^4p^4)$. The operators have been normalized such that $c_i = 1$ at tree level. The one-loop radiative corrections to c_1, c_5 and c_6 have been reported in [2]. We can also add further spin-dependent interaction terms to obtain the “full spin v^6 NRQCD” action given by

$$\begin{aligned} \delta H_{v^6} = & -f_1 \frac{g}{8M^3} \left\{ \Delta^{(2)}, \boldsymbol{\sigma} \cdot \tilde{\mathbf{B}} \right\} \\ & - f_2 \frac{3g}{64M^4} \left\{ \Delta^{(2)}, \boldsymbol{\sigma} \cdot \left(\tilde{\mathbf{\Delta}}^{(\pm)} \times \tilde{\mathbf{E}} - \tilde{\mathbf{E}} \times \tilde{\mathbf{\Delta}}^{(\pm)} \right) \right\} \\ & - f_3 \frac{ig^2}{8M^3} \boldsymbol{\sigma} \cdot \tilde{\mathbf{E}} \times \tilde{\mathbf{E}}, \end{aligned} \quad (5)$$

where again the operators have been normalized such that at tree-level $f_i = 1$.

The unimproved forward and backward derivatives are defined by

$$\begin{aligned} (\Delta_\mu^+ f)(x) &= \frac{1}{a} (U_\mu(x) f(x + \hat{\mu}) - f(x)), \\ (\Delta_\mu^- f)(x) &= \frac{1}{a} (f(x) - U_{-\mu}(x) f(x - \hat{\mu})), \end{aligned} \quad (6)$$

and the unimproved higher order lattice derivatives are

$$\Delta^{(2n)} = \sum_{j=1}^3 (\Delta_j^{(+)} \Delta_j^{(-)})^n. \quad (7)$$

The $O(a^4p^4)$ -improved symmetric derivative is given by

$$\tilde{\Delta}^{(\pm)} = \Delta_j^{(\pm)} - \frac{1}{6} \Delta_j^{(+)} \Delta_j^{(\pm)} \Delta_j^{(-)}. \quad (8)$$

$\tilde{\mathbf{B}}$ and $\tilde{\mathbf{E}}$ are the improved chromomagnetic and chromoelectric fields, constructed from standard cloverleaf

operators, and improved to $O(a^2)$:

$$\tilde{B}_k = -\frac{1}{2} \epsilon_{klm} F_{lm}^{imp}, \quad (9)$$

$$\tilde{E}_k = F_{k4}^{imp}, \quad (10)$$

$$F_{\mu\nu}^{imp} = \frac{5}{3} F_{\mu\nu} - \frac{1}{6} [U_\mu F_{\mu\nu} U_\nu^\dagger + U_\mu^\dagger F_{\mu\nu} U_\nu + (\mu \leftrightarrow \nu)], \quad (11)$$

$$F_{\mu\nu} = -\frac{i}{2g} (I_{\mu\nu} - I_{\mu\nu}^\dagger), \quad (12)$$

$$\begin{aligned} I_{\mu\nu} = & \frac{1}{4} \sum_{\{(\alpha, \beta)\}_{\mu\nu}} U_\alpha(x) U_\beta(x + \hat{\alpha}) U_{-\alpha}(x + \hat{\alpha} + \hat{\beta}) U_{-\beta}(x + \hat{\beta}), \end{aligned} \quad (13)$$

where $\{(\alpha, \beta)\}_{\mu\nu} = (\mu, \nu), (\nu, -\mu), (-\mu, -\nu), (-\nu, \mu)$ for $\mu \neq \nu$.

Mean-field (tadpole) improvement is implicitly included in the definition of the links by replacing $U_\mu \mapsto U_\mu / \langle u_0 \rangle$, where u_0 is the Landau gauge mean link. Since the gauge links are unitary, some of the correction terms in F^{imp} will be only four, rather than six, links long due to cancellations of the form $U_\mu U_\mu^\dagger$, and so should carry a factor of $\frac{1}{u_0^4}$ (rather than $\frac{1}{u_0^6}$). This is implemented by the addition of a further correction term [35] and must be taken into account when calculating mean-field improvement contributions.

IV. CHROMOMAGNETIC INTERACTION

The hyperfine splitting of S-wave bottomonium, $M_\Upsilon - M_{\eta_b}$, provides a high-precision test of NRQCD [5]. The size of the hyperfine splitting is expected to be approximately proportional to the square of the coefficient c_4 of the chromomagnetic operator in the NRQCD action. While most NRQCD simulations so far have set $c_4 = 1$, this coefficient will receive radiative corrections at $O(\alpha_s)$, which have the potential of affecting the predicted value for the hyperfine splitting significantly, so that without a determination of these radiative corrections, large systematic errors have to be included in any NRQCD calculation of the hyperfine splitting. For example, in [1] the ground state hyperfine splitting is predicted to be $M_\Upsilon - M_{\eta_b} = 61(14) MeV$, where the dominant errors are from the missing $O(\alpha_s)$ corrections to c_4 . This prediction is smaller than the experimental value of $M_\Upsilon - M_{\eta_b} = 71.4(+2.3)(-3.1)(3.7)$, [36] although within the large theoretical errors, theory and experiment agree.

At the one-loop level, the contributions to the effective action relevant for determining the chromomagnetic operator arise from the vertex diagrams shown in Figure 1. As the QCD analogue of the magnetic moment operator in QED, the chromomagnetic moment operator constitutes the leading contribution to the hyperfine splitting within hadronic states, and by tuning of the coefficient c_4

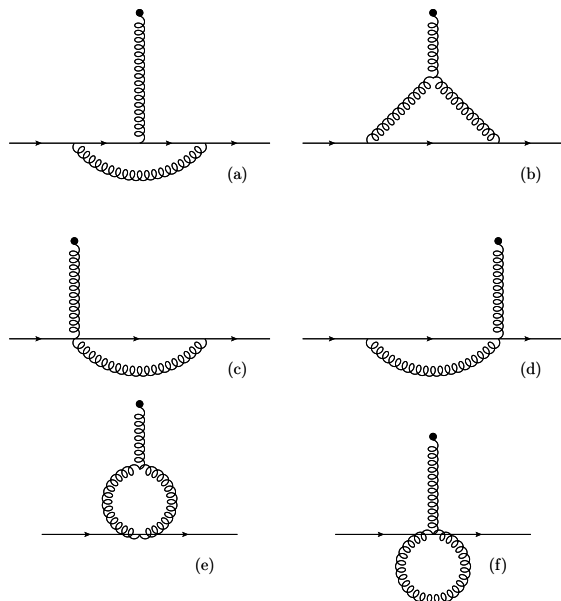


FIG. 1. Vertex correction Feynman diagrams. Referred to as (a) QED (b) nonabelian (c)&(d) swordfish (e) algae (f) ankh diagrams.

of the chromomagnetic operator in the NRQCD action, we can match NRQCD to QCD as far as the hyperfine splitting is concerned.

In this section we compute the radiative improvement correction to c_4 which takes the form $c_4 = 1 + \alpha_s c_4^{(1)}$ with $c_4^{(1)} = A + B \log(Ma)$, where a is the lattice spacing, M is the heavy quark mass, and A and B are constants which we calculate. In continuum QCD, all corrections can be computed analytically following standard techniques; for the calculation in lattice NRQCD, we employ the automated Feynman rule packages HPSRC and HiPPY [37].

A. Continuum QCD Calculation

The QCD effective action contains the following terms bi-linear in the fermionic fields,

$$\Gamma^{QCD} = Z_2^{-1} \bar{\Psi}(\not{\partial} + \not{A})\Psi + \delta Z_\sigma \bar{\Psi} \frac{\sigma^{\mu\nu} F_{\mu\nu}}{2m} \Psi + \dots, \quad (14)$$

where, because of BFG invariance, the matter terms and $\bar{\Psi} \not{A} \Psi$ vertex are packaged into a gauge covariant derivative so as to obey the Slavnov-Taylor identity $Z_{1F} = Z_2^{-1}$. The constants Z are thus related to the usual chromodynamic form factors via $Z_{1F} = F_1(0)$ and $\delta Z_\sigma = F_2(0)$. The first term is multiplicatively renormalized to

$$\bar{\Psi}_R(\not{\partial} + \not{A})\Psi_R, \quad (15)$$

and BFG ensures that A is not renormalized. The second term renormalizes to

$$b_\sigma \bar{\Psi}_R \frac{\sigma^{\mu\nu} F_{\mu\nu}}{2m_R} \Psi_R, \quad (16)$$

with

$$b_\sigma = Z_\sigma Z_2 Z_m. \quad (17)$$

Since QCD is renormalizable, the absence of a Pauli term in the bare QCD action ensures that b_σ is UV finite; it moreover implies that $Z_\sigma = O(\alpha_s)$, so that to leading order we can set $Z_2 = Z_m = 1$.

After performing a non-relativistic reduction using a Foldy-Wouthuysen-Tani (FWT) transformation [38, 39], Eqs. (15) and (16) reduce to

$$(1 + b_\sigma) g \psi_R^\dagger \frac{\boldsymbol{\sigma} \cdot \mathbf{B}}{2m_R} \psi_R, \quad (18)$$

where B is the chromomagnetic field. It is worth noting the relationship between various notations for these renormalization constants: at the one loop level

$$1 + b_\sigma = 1 + Z_\sigma Z_2 = (F_1(0) + F_2(0))Z_2 = G_M(0)Z_2. \quad (19)$$

Note that there is no factor of Z_m in these expressions, since the Gordon decomposition of the tree-level $\bar{\Psi} \not{A} \Psi$ term is between on-shell spinors and so we automatically have the renormalized mass in the resulting chromomagnetic term. As stated before, b_σ is UV finite; this is crucial for our analysis, since it enables us to directly equate results obtained on the lattice to those obtained in the continuum since the difference between the schemes for UV regulation is then irrelevant.

The two diagrams contributing to b_σ are given in Figure 1 (a) and (b), and we introduce a small gluon mass μ as an IR regulator. A straightforward analytic calculation then gives

$$b_\sigma = \frac{3\alpha_s}{2\pi} \log \frac{\mu}{m} + \frac{13\alpha_s}{6\pi}, \quad (20)$$

at one loop. This continuum calculation was verified using the HiPPY and HPSRC packages by reproducing the same result numerically in the limit $ma \rightarrow 0$; in this way it was also confirmed that the result was gauge-parameter independent. Note that the choice of BFG was crucial to ensure a UV finite result.

B. NRQCD Calculation

The leading spin-dependent term in the effective action for NRQCD is

$$\Gamma^{\text{NRQCD}} = c_4 Z_\sigma^{\text{NR}} g \psi^\dagger \frac{\boldsymbol{\sigma} \cdot \mathbf{B}}{2M} \psi + \dots, \quad (21)$$

which, after renormalization, becomes

$$\Gamma^{\text{NRQCD}} = c_4 Z_\sigma^{\text{NR}} Z_2^{\text{NR}} Z_m^{\text{NR}} \psi_R^\dagger \frac{\boldsymbol{\sigma} \cdot \mathbf{B}}{2M_R} \psi_R. \quad (22)$$

Since the chromomagnetic operator is present in the NRQCD action at tree level, Z_σ is of the form $Z_\sigma^{\text{NR}} =$

$1 + Z_\sigma^{\text{NR},(1)}\alpha_s$. Requiring that the anomalous chromomagnetic moment to be equal in QCD and NRQCD, we obtain the matching condition

$$c_4 Z_\sigma^{\text{NR}} Z_2^{\text{NR}} Z_m^{\text{NR}} = 1 + Z_\sigma, \quad (23)$$

which at tree level and one-loop order yields

$$\begin{aligned} c_4^{(0)} &= 1, \\ c_4^{(1)} &= b_\sigma^{(1)} - Z_\sigma^{\text{NR},(1)} - Z_2^{\text{NR},(1)} - Z_m^{\text{NR},(1)}. \end{aligned} \quad (24)$$

Note that mass renormalization has to be included in NRQCD since the chromomagnetic operator is now included at tree-level.

All of the renormalization constants involved are UV finite and consist of two distinct contributions: besides the ordinary diagrammatic contributions (which we denote simply as Z), there are also contributions from mean-field improvement (Z^{tad}). The NRQCD diagrams contributing to $Z_\sigma^{\text{NR},(1)}$ are shown in Figure 1 (a)-(e). Note that diagrams (c)-(e) receive contributions not only from lattice artifacts, but also from higher-adicity vertices that are also present in continuum NRQCD.

Having once coded the Feynman diagrams in Figure 1 using the HPSRC package, we can repeat the numerical evaluation of these diagrams for each NRQCD action of interest by using the HIPPY package to automatically generate Feynman rules for that action along with the Symanzik-improved gluonic action.

By using the residual gauge-invariance of the effective potential in BFG, the contribution to the negative of the effective action from the diagrams can be restricted to the form

$$\begin{aligned} & -\delta\Gamma_{\bar{\psi}\psi A_i}(p, q) = \\ & -Z_\sigma^{\text{NR},(1)} g\psi(p+q)^\dagger \frac{i\epsilon_{ijk}\sigma_j q_k A_i(q)}{2M} \psi(p) + \dots, \end{aligned} \quad (25)$$

where $i = 1, 2, 3$ and terms of higher order in the external momentum q have been omitted. Without BFG, non-gauge invariant operators would be generated as counterterms, greatly increasing the difficulty of the calculation and the subsequent use of the improved action in simulations. Using the automatic differentiation [40, 41] and spinor manipulation facilities built into the HPSRC package, the coefficient of interest can be isolated as

$$Mi \frac{\partial}{\partial p_1} \text{Tr} (\delta\Gamma_{\bar{\psi}\psi A_2}(p, 0)\sigma_3) = gZ_\sigma^{\text{NR},(1)}, \quad (26)$$

where $\mathbf{p} = 0$, with p_0 taken such that the quark is on-shell using the lattice equation of motion as implemented in the HPSRC package.

We integrate over the temporal component k_4 of the loop momentum k by contour integration over the unit circle $w = e^{ik_4}$ in the complex plane. The positions of the poles in the integrand arising from the gluon and quark propagators in the Feynman diagram are functions of the spatial loop momentum \mathbf{k} . To ensure that no poles

cross the contour of integration as \mathbf{k} varies, we change the contour to be a circle of radius r , choosing r such that the contour lies exactly half-way between the outermost interior pole and the innermost exterior pole. Since there are no physical intermediate states and thus no branch cut in any of the diagrams this strategy is always possible [42]. Since it is known that the poles of full NRQCD and improved gluonic actions always lie further away from the contour than their unimproved counterparts [43], it is therefore safe to reduce the effort by locating the poles corresponding to the unimproved action and shift the contour appropriately.

The renormalization constants

$$Z_2^{\text{NR},(1)} = 1 + \text{Re}\Sigma(0) + \text{Im} \left. \frac{\partial\Sigma}{\partial p_4} \right|_{p=0}, \quad (27)$$

$$Z_m^{\text{NR},(1)} = 1 + M \text{Re} \left. \frac{\partial^2\Sigma}{\partial p_3^2} \right|_{p=0} - \text{Im} \left. \frac{\partial\Sigma}{\partial p_4} \right|_{p=0}, \quad (28)$$

are determined from the quark self-energy $-\Gamma_{\bar{\psi}\psi}(-p, p) = \Sigma(p)$, which is given by the diagrams shown in Figure 2.

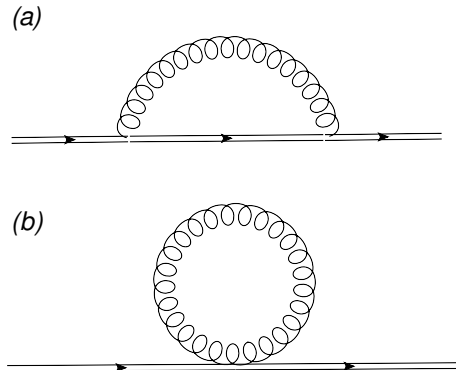


FIG. 2. Quark two-point function Feynman diagrams. Referred to as (a) rainbow and (b) tadpole diagrams.

Both $Z_2^{\text{NR},(1)}$ and $Z_\sigma^{\text{NR},(1)}$ contain logarithmic IR divergences. For our purposes, it sufficient to evaluate their sum for which the IR logarithm is known from analytical results. We can therefore determine the IR finite diagrammatic contribution \tilde{Z}_X from fitting our numerical results with the form

$$Z_\sigma^{\text{NR},(1)} + Z_2^{\text{NR},(1)} = \tilde{Z}_\sigma^{\text{NR},(1)} + \tilde{Z}_2^{\text{NR},(1)} + \frac{3}{2\pi} \log \mu a. \quad (29)$$

We evaluate the diagrams for $10^{-8} < \mu < 10^{-6}$ such that any $(\mu a)^2$ lattice artifacts can be neglected in the fit. The logarithmic IR divergence combines with the IR logarithm from the QCD result above to yield an overall logarithmic contribution $-\frac{3\alpha_s}{2\pi} \log(Ma)$ to $c_4^{(1)}$.

$Z_\sigma^{\text{NR},(1)}$ and $Z_m^{\text{NR},(1)}$ also receive corrections from tadpole improvement, whereas there are no tadpole corrections to $Z_2^{\text{NR},(1)}$. Using a MATHEMATICA [44] notebook developed in the course of earlier related work [42, 45],

the tadpole corrections are determined by symbolically substituting mean field corrections, $U \rightarrow U/u_0$ with $u_0 = 1 - \alpha_s u_0^{(2)}$, into the NRQCD action. The tadpole corrections are dependent on the details of the NRQCD action used, in particular also on the value of the stability parameter n .

For the full v^4 NRQCD action we find

$$Z_m^{\text{tad},(1)} = - \left(\frac{2}{3} + \frac{3}{(Ma)^2} \right) u_0^{(2)}. \quad (30)$$

The tadpole contribution to $Z_\sigma^{\text{NR},(1)}$ arises from two sources: the application of mean-field improvement to the improved field-strength tensor, and the cross-multiplication of the tree-level $\sigma \cdot \mathbf{B}$ term with the tadpole corrections terms in H_0 [1]. The overall result for the full v^4 NRQCD action is

$$Z_\sigma^{\text{tad},(1)} = \left(\frac{13}{3} + \frac{13}{4Ma} - \frac{3}{8n(Ma)^2} - \frac{3}{4(Ma)^3} \right) u_0^{(2)}. \quad (31)$$

We take the one-loop contribution to the Landau mean link to be $u_0^{(2)} = 0.750$ [46].

C. Results

The final result for the radiative correction to c_4 is given by

$$c_4^{(1)} = \frac{13}{6\pi} - \tilde{Z}_\sigma^{\text{NR},(1)} - \tilde{Z}_2^{\text{NR},(1)} - \tilde{Z}_m^{\text{NR},(1)} - Z_m^{\text{tad},(1)} - Z_\sigma^{\text{tad},(1)} - \frac{3}{2\pi} \log Ma. \quad (32)$$

Results for several different NRQCD actions, all used with the tree-level Symanzik gluon action, are summarized in Tables I-III. The values of Ma were chosen to correspond to the lattice spacings for lattices used by the HPQCD collaboration [1].

We note that the tadpole corrections to Z_σ and Z_m in each case very nearly cancel the diagrammatic contribution, demonstrating that they are working as intended by reducing the coefficient of α_s in the perturbative series. Without such a tadpole correction we find $c_4^{(1)} \approx 4$, meaning that the viability of the perturbative expansion would be highly questionable.

On the other hand, the radiative corrections for the full v^4 NRQCD action with stability parameter for $n = 2$ or $n = 4$ differ very little; in the case of the full spin v^6 NRQCD action it appears that for small values of Ma the correction increases slightly, but for larger values of Ma the corrections are very similar to the v^4 case. These results suggest that the radiative corrections for the chromomagnetic operator are relatively independent of the details of the NRQCD action.

Note that for all actions and ranges of Ma the total correction is positive: the constant part of the correction is larger than the (negative) logarithmic contribution. This refutes the claims of Penin [47], who does not include a

calculation of the Ma -independent constant contribution to $c_4^{(1)}$ which is responsible for $c_4^{(1)}$ being positive.

In Figure 3 we plot the dependence of the radiative correction $c_4^{(1)}$ against Ma for full NRQCD $n = 4$. While the expected divergence in the $Ma \rightarrow 0$ limit can be seen, for values of $2 < Ma < 4$ the correction varies only slowly, demonstrating that for the range of lattice spacings used by the HPQCD collaboration the perturbative improvement corrections are under control.

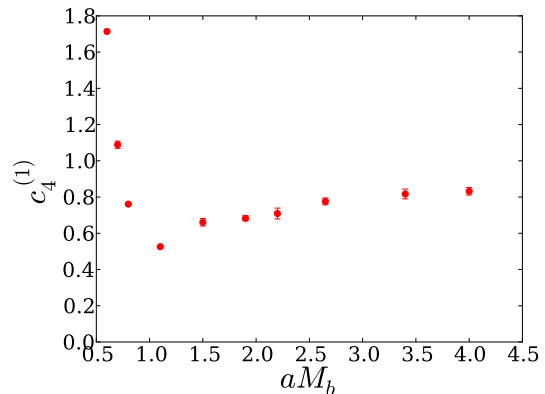


FIG. 3. Lattice spacing dependence for the chromomagnetic operator correction, full $O(v^4)$ NRQCD $n = 4$ action.

Ma	1.95	2.8	4.0
$\tilde{Z}_\sigma^{(1)} + \tilde{Z}_2^{(1)}$	-5.164(7)	-4.913(6)	-4.739(6)
$\tilde{Z}_m^{(1)}$	1.512(1)	1.022(3)	0.723(2)
$Z_\sigma^{\text{tad},(1)}$	4.387	4.077	3.841
$Z_m^{\text{tad},(1)}$	-1.092	-0.787	-0.641
$c_4^{(1)}$	0.728(7)	0.799(7)	0.842(6)

TABLE I. Renormalization parameters for the chromomagnetic term, full v^4 NRQCD $n = 2$

Ma	1.9	2.65	3.4
$\tilde{Z}_\sigma^{(1)} + \tilde{Z}_2^{(1)}$	-5.17(1)	-4.94(1)	-4.80(2)
$\tilde{Z}_m^{(1)}$	1.56(1)	1.08(1)	0.84(1)
$Z_\sigma^{\text{tad},(1)}$	4.43	4.129	3.95
$Z_m^{\text{tad},(1)}$	-1.12	-0.82	-0.69
$c_4^{(1)}$	0.68(1)	0.78(2)	0.82(3)

TABLE II. Renormalization parameters for the chromomagnetic term, full v^4 NRQCD $n = 4$

V. THE DARWIN OPERATOR

The vertex correction diagrams of Figure 1 also renormalize the $\mathbf{D} \cdot \mathbf{E}$ operator (conventionally called the Darwin term in analogy with atomic physics) in the effective

Ma	1.9	2.65	3.4
$\tilde{Z}_\sigma^{(1)} + \tilde{Z}_2^{(1)} + \tilde{Z}_m^{(1)}$	-4.33(8)	-4.16(7)	-4.16(5)
$Z_\sigma^{\text{tad},(1)} + Z_m^{\text{tad},(1)}$	3.93	3.63	3.45
$c_4^{(1)}$	0.78(8)	0.76(7)	0.83(5)

TABLE III. Renormalization parameters for the chromomagnetic term, full spin v^6 NRQCD $n = 4$

action. The primary effect of this operator is to change the effective potential for the wavefunction at the origin; since only states with $L = 0$ have a non-vanishing wavefunction at the origin, this results in an energy shift for S-wave states.

In the same manner as for the chromomagnetic operator, we can tune the coefficient c_2 of the Darwin term so as to correct for the difference between the loop corrections of QCD and NRQCD. Previously, these corrections were unknown, and the coefficient c_2 has been set equal to one in most non-perturbative simulations so far. While non-perturbative studies have shown a comparatively mild dependence of energy levels on varying the value of c_2 [2], a precise determination of the radiative corrections to c_2 is a logical continuation of our improvement programme.

A. Continuum QCD Calculation

In continuum QCD, we need to consider the q^2 -dependence of the effective action,

$$\Gamma^{QCD} = \bar{\Psi} F_1(q^2) \not{A} \Psi + \bar{\Psi} \frac{F_2(q^2) \sigma^{\mu\nu} F_{\mu\nu}}{2m} \Psi + \dots, \quad (33)$$

where for the chromomagnetic case we had $F_1(0) = Z_{1F} (= Z_2^{-1})$ and $F_2(0) = Z_\sigma$. Upon performing the non-relativistic reduction and isolating the terms containing the time component A_0 of the gauge field, we find

$$\begin{aligned} \Gamma^{QCD} = & F_1(q^2) \psi^\dagger \left[gA_0 - \frac{g}{8m^2} q^2 A_0 + \dots \right] \psi \\ & + F_2(q^2) \psi^\dagger \left[-\frac{g}{4m^2} q^2 A_0 + \dots \right] \psi, \end{aligned} \quad (34)$$

which, after renormalization, gives the Darwin term as

$$\begin{aligned} \Gamma^{QCD} = & \\ & [1 - 8m^2 F_1'(0) + 2F_2(0)] \psi_R^\dagger \left[-\frac{g}{8m_R^2} q^2 A_0 \right] \psi_R + \dots \end{aligned} \quad (35)$$

Note that F_2 contributes through the non-relativistic reduction, whereas F_1 only contributes through its expansion around $q^2 = 0$, since the wavefunction renormalization cancels any contribution from $F_1(0)$. Again, we do not have to include mass renormalization since the renormalized mass m naturally appears when using the non-relativistic reduction between on-shell spinors.

$F_2(0)$ has already been computed for the chromomagnetic case. For the contribution from the abelian diagram of Figure 1(a), one finds

$$F'_{1a}(0) = \frac{\alpha_s}{8m^2} \left[-\frac{1}{6\pi} - \frac{4}{9\pi} \log \mu/m \right], \quad (36)$$

and for the non-abelian diagram of Figure 1(b) we may take the derivative of the analytical calculation carried out for the chromomagnetic term to obtain

$$F'_{1b}(0) = \frac{\alpha_s}{8m^2} \left[\frac{m^2}{\mu^2\pi} + \frac{7m}{4\mu} + \frac{11}{2\pi} + \frac{9}{\pi} \log \mu/m \right]. \quad (37)$$

The total contribution to the continuum QCD Darwin term is then

$$Z_D = 1 + \alpha_s \left[-\frac{m^2}{\mu^2\pi} - \frac{7m}{4\mu} - \frac{1}{\pi} + \left(-\frac{6}{\pi} + \frac{4}{9\pi} \right) \log \mu/m \right], \quad (38)$$

where as before, we use a gluon mass μ as the IR regulator. We note, however, that the case of the Darwin term is more subtle since there are power-law IR divergences which will have to match and cancel with corresponding IR divergences on the NRQCD side.

B. NRQCD Calculation

The Darwin term in the NRQCD effective action is given by

$$\Gamma^{\text{NRQCD}} = -c_2 Z_D^{\text{NR}} g \psi^\dagger \frac{q^2 A_0}{8M^2} \psi + \dots \quad (39)$$

where again Z_D^{NR} has a tree-level contribution, $Z_D^{\text{NR}} = 1 + Z_D^{\text{NR},(1)} \alpha_s + \dots$. After renormalization we obtain,

$$\Gamma^{\text{NRQCD}} = -c_2 Z_D^{\text{NR}} (Z_m^{\text{NR}})^2 Z_2^{\text{NR}} g \psi_R^\dagger \frac{q^2 A_0}{8M_R^2} \psi_R + \dots \quad (40)$$

Requiring the coefficients of the Darwin term to be equal in QCD and NRQCD, we find the matching condition

$$c_2 Z_D^{\text{NR}} Z_2^{\text{NR}} (Z_m^{\text{NR}})^2 = Z_D, \quad (41)$$

which at tree level and one-loop order gives

$$\begin{aligned} c_2^{(0)} &= 1, \\ c_2^{(1)} &= Z_D^{(1)} - Z_D^{\text{NR},(1)} - Z_2^{\text{NR},(1)} - 2Z_m^{\text{NR},(1)}. \end{aligned} \quad (42)$$

As in the chromomagnetic case, the diagrammatic contributions, labelled as Z , must be supplemented by the corresponding mean-field corrections, Z^{tad} .

Again, the symmetries of the effective action in BFG restrict the form of the diagrammatic contributions to

$$-\delta\Gamma_{\bar{\psi}\psi A_0}(p, q) = -Z_D^{\text{NR},(1)} g \psi(p+q)^\dagger \frac{q^2 A_0(q)}{8M} \psi(p) + \dots \quad (43)$$

Working in the Breit frame ($p_i = -q_i/2$) for ease of implementation, we isolate the renormalization constant

$$Z_D^{\text{NR},(1)} = -\frac{4M^2}{3} \sum_i \frac{\partial^2}{\partial q_i^2} \delta\Gamma_{\bar{\psi}\psi A_0}(0,0) - M \frac{\partial}{\partial p_0} \delta\Gamma_{\bar{\psi}\psi A_0}(0,0), \quad (44)$$

where the second term arises from the on-shell condition of the incoming and outgoing quarks. We note that the final result is of course independent of the choice of frame used.

By taking advantage of the modular structure of the HIPPY and HPSRC packages, we are able to reuse the same code that we used for matching the chromomagnetic operator by merely changing the incoming gauge field Lorentz index to isolate the A_0 component, and taking the trace of the diagram to isolate the implicit Dirac unit matrix in front of the Darwin operator. The pole structure for each individual diagram remains as in the previous calculations.

The presence of severe IR divergences in some of the diagrams makes it necessary to analytically identify and subtract those divergences, leaving only the IR finite

piece \tilde{Z} to be computed numerically. For the sake of brevity, the superscript NR is suppressed in the remainder of this section except where it is necessary to avoid confusion.

For the diagram in Figure 1(a) we obtain

$$Z_D^{a,(1)} = \tilde{Z}_D^{a,(1)} + \left[\frac{4}{9\pi} - \left(\frac{1}{6\pi} \right) \right] \log \mu a, \quad (45)$$

where the IR divergence in round brackets arises from the inclusion of the tree-level Darwin term in the action. We therefore would expect this divergence to be cancelled by an IR divergence in the wavefunction renormalization times the tree-level operator. Since the IR divergences are calculated analytically we can use a constrained fit to find the constant μa -independent contribution, $\tilde{Z}_D^{(a),(1)}$.

For the diagram in Figure 1(b) we have

$$Z_D^{(b),(1)} = \tilde{Z}_D^{(b),(1)} + D(Ma) \log \mu a - \frac{7M}{4\mu} - \frac{M^2}{\pi\mu^2}, \quad (46)$$

where $D(Ma)$ is an action-specific coefficient containing lattice artifacts. The leading continuum power-law divergences are removed by the subtraction function

$$I^{\text{sub}}(\mu) = (4\pi)(8M^2) \int \frac{d^4k}{(2\pi)^4} \left[\frac{\frac{7}{8M}}{(k^2 + \mu^2)^2 (ik_0 + k^2/2M)} + \frac{(3\mu^2)}{(k^2 + \mu^2)^4} \right] = \tilde{Z}^{\text{sub},(1)} + \frac{7M}{4\mu} + \frac{21}{4\pi} \log \mu a + \frac{M^2}{\pi\mu^2} + P^{\text{sub}}(\mu a), \quad (47)$$

where $P^{\text{sub}}(\mu a)$ is a polynomial in μa with $P^{\text{sub}}(0) = 0$. This subtraction function is chosen to cancel the leading M^2/μ^2 and M/μ IR divergences pointwise and also contains a continuum-like IR log divergence which is shown in Eq. (47). We calculate $\tilde{Z}^{\text{sub},(1)}$ from a fit to $I^{\text{sub}}(\mu)$, using values of the cutoff in the range $10^{-3} < \mu < 10^{-1}$ and fitting the results to a polynomial in μa . In Figure 4 we show a typical fit for the subtraction function giving the required renormalization constant \tilde{Z}^{sub} . From the figure we note that the magnitude of the error increases as μ decreases and the cost of computation correspondingly increases.

In addition to containing continuum IR divergences, the graph in Figure 1(b) contains additional artifact logarithmic IR divergences in NRQCD which must ultimately cancel against similar contributions from the graphs in Figure 1(c-f). We calculate these diagrams, namely the swordfish, algae, and ankh diagrams, and add their contribution to that of the subtracted diagram in Figure 1(b) to compute the overall logarithmic IR divergence which should not (and indeed does not) contain a lattice artefact IR logarithm.

For the swordfish, algae and ankh diagrams we write

$$Z_D^{c-f,(1)} = \tilde{Z}_D^{c-f,(1)} + D'(Ma) \log \mu a, \quad (48)$$

where $D'(Ma)$ is the action-specific coefficient of the lattice artefact logarithmic IR divergence. We find that

$$D(Ma) + D'(Ma) = -\frac{6}{\pi} + \left(\frac{3}{2\pi} \right), \quad (49)$$

which is independent of lattice artifacts, as expected. As before, the term in round brackets arises from the inclusion of the tree-level Darwin term in the NRQCD action. The graphs in Figure 1(b-f) are combined with the subtraction function in Eq. (47) and the integral computed numerically. Combining the diagrams in Figure 1(b-f) we compute, as a function of μa , the combination

$$Z_D^{b,(1)} + I^{\text{sub}} - \tilde{Z}^{\text{sub},(1)} + Z_D^{c-f,(1)} = \tilde{Z}^{b,(1)} + \tilde{Z}^{c-f,(1)} + \frac{3}{4\pi} \log \mu a + P^{b-f}(\mu a), \quad (50)$$

where $P^{b-f}(\mu a)$ is a polynomial in μa with $P^{b-f}(0) = 0$, and the fit to the parameterization with the coefficient

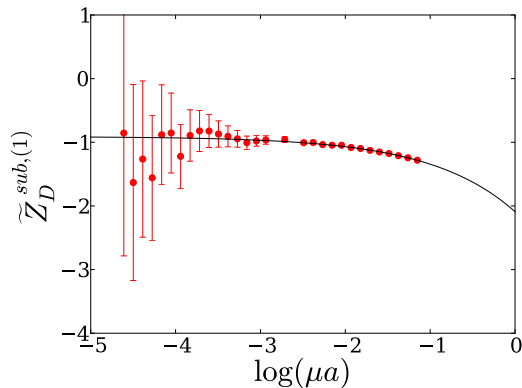


FIG. 4. Sample fit for $\tilde{Z}_D^{sub,(1)}$. $Ma = 1.9$. We obtain $-0.91(1) - 1.18(5)\mu a$ with $\chi^2/d.o.f. = 0.21$.

of the logarithmic IR divergence constrained to its analytic value gives a much better estimate for the required renormalization constants.

The presence of the tree-level Darwin term in the NRQCD action means we have also to include the con-

$$c_2^{(1)} = -\frac{1}{\pi} - \tilde{Z}^{b,(1)} - \tilde{Z}^{c-f,(1)} - \tilde{Z}^{a,(1)} - Z_D^{tad,(1)} - \tilde{Z}_2^{(1)} - 2Z_m^{(1)} - 2Z_m^{tad,(1)} + \frac{50}{9\pi} \log Ma, \quad (53)$$

where again the logarithmic divergences in NRQCD and QCD have combined to give a term proportional to $\log Ma$.

C. Results

In Tables IV and V we give results for the full v^4 NRQCD action and the full spin v^6 NRQCD action respectively, both with stability parameter $n = 4$. For brevity, we use the notation

$$\tilde{Z}^{a-f,(1)} = \tilde{Z}^{a,(1)} + \tilde{Z}^{b,(1)} + \tilde{Z}^{c-f,(1)}. \quad (54)$$

Again, we find that the tadpole correction cancels the major part of the diagrammatic contribution to $c_2^{(1)}$, indicating improved convergence of the resulting perturbative series. This effect is expected and reinforces the efficacy of including tadpole improvement.

Numerical simulations [2] show that using a value of $c_2 = 1.25$ shifts the energy of the $\Upsilon(1S)$ state by less than

tribution from the wavefunction renormalization

$$Z_2^{NR,(1)} = \tilde{Z}_2^{(1)} - \frac{4}{3\pi} \log \mu a. \quad (51)$$

As expected, the IR logarithm in Z_2 does indeed cancel the sum of the logarithmic IR divergences displayed in round brackets in Eqs. (45) and (49).

The mass renormalization is finite and so can be simply added to the result.

As for the chromomagnetic term, we must also include tadpole contributions, which in this case come from three sources: the improvement of the field strength tensor, the improvement of $\nabla^{(\pm)}$, and from cross-multiplication with tadpole-improved links in the other parts of the NRQCD action. Altogether, this gives

$$\delta Z_D^{tad} = \left(\frac{16}{3} - \frac{3}{4M^3} - \frac{3}{32M^2} + \frac{13}{4M} \right) u_0^{(2)}, \quad (52)$$

which is the same as the tadpole correction to the chromomagnetic term plus 1 from the correction of $\nabla^{(\pm)}$. The mass renormalization tadpole is the same as used in the chromomagnetic calculation.

All lattice artefact IR divergences cancel internally within the NRQCD calculation and the continuum IR log divergences match between the continuum and lattice NRQCD calculations. Using the result for the continuum contribution in Eq. (38) and summing all lattice NRQCD contributions, we find the one-loop improvement coefficient for the NRQCD Darwin term to be

one percent compared with the tree-level value $c_2 = 1$, indicating that the radiative corrections are well under control.

Ma	$\tilde{Z}^{a-f,(1)}$	$Z_D^{tad,(1)}$	$c_2^{(1)}$	α_V	c_2
1.9	-5.95(8)	5.18	1.33(8)	0.22	1.29(2)
2.65	-3.71(10)	4.88	0.08(10)	0.25	1.02(3)
3.4	-1.73(12)	4.69	-1.20(12)	0.27	0.68(4)

TABLE IV. Renormalization parameters for the Darwin term, full v^4 NRQCD $n = 4$

VI. FOUR-FERMION INTERACTIONS

At the one-loop level, calculations in NRQCD must also take account of four-fermion interactions in the NRQCD action that are needed to match $QQ \rightarrow QQ$ scattering processes between QCD and NRQCD. While

Ma	$\tilde{Z}^{a-f,(1)}$	$Z_D^{tad,(1)}$	$c_2^{(1)}$	α_V	c_2
1.9	-5.83(8)	5.18	1.32(9)	0.22	1.29(2)
2.65	-3.64(10)	4.88	0.10(10)	0.25	1.03(3)
3.4	-1.67(11)	4.69	-1.23(11)	0.27	0.67(4)

TABLE V. Renormalization parameters for the Darwin term, full spin v^6 NRQCD $n = 4$

so far we have emphasized the rôle of the effective action in BFG, the matching condition must ultimately equate physical, on-shell matrix element, which in general will include contributions from 1PR diagrams, and so it is not necessarily possible to match just the effective actions term by term.

A. Formalism

The radiatively generated four-fermion interactions that need to be added to the NRQCD action can be written as four-fermion contact operators in a (covariant) derivative expansion. Here we consider only the lowest-order terms in this expansion, namely those without derivatives. One obvious set of operators which bear a close relationship to the $\bar{Q}Q \rightarrow \bar{Q}Q$ diagrams calculated, is given by

$$\begin{aligned}
S^{NRQCD} = & \\
& a_8 \frac{\alpha_s g^2}{M^2} (\chi^\dagger T_a^T \chi) (\psi^\dagger T_a \psi) + a_1 \frac{\alpha_s g^2}{M^2} (\chi^\dagger \chi) (\psi^\dagger \psi) \\
& + b_8 \frac{\alpha_s g^2}{M^2} (\chi^\dagger \sigma^* T_a^T \chi) (\psi^\dagger \sigma T_a \psi) + b_1 \frac{\alpha_s g^2}{m^2} (\chi^\dagger \sigma^* \chi) (\bar{\psi} \sigma \psi).
\end{aligned} \tag{55}$$

We will refer to the operators with coefficients a_1 and b_1 as singlet-exchange operators. The operators with coefficients a_8 and b_8 , which we will refer to as octet-exchange operators, give corrections to processes involving single gluon exchange at tree level. This relation will be useful later when discussing corrections to the QCD Coulomb force. The spin-independent and spin-dependent operators have coefficients a_i and b_i , $i = 1, 8$, respectively. Only b_1 and b_8 will contribute to the hyperfine splitting, as can be seen by choosing the more conventional set of operators given by [4, 8]

$$\begin{aligned}
S^{NRQCD} = & d_1 \frac{\alpha_s^2}{M^2} (\psi^\dagger \chi^*) (\chi^T \psi) + d_2 \frac{\alpha_s^2}{M^2} (\psi^\dagger \sigma \chi^*) (\chi^T \sigma \psi) \\
& + d_3 \frac{\alpha_s^2}{M^2} (\psi^\dagger T_a \chi^*) (\chi^T T_a \psi) + d_4 \frac{\alpha_s^2}{M^2} (\psi^\dagger \sigma T_a \chi^*) (\chi^T \sigma T_a \psi).
\end{aligned} \tag{56}$$

Here, we choose the χ field for the antiquark to transform according to the conjugate $\bar{1}/2$ representation of spin and the $\bar{3}$ representation of colour generated, respectively, by $-\sigma^*$ and $-T^*$. Such s-channel operators make explicit

their effects on different meson states; this will be useful in later discussions of the hyperfine splitting.

These two sets of operators in Eqs. (55), (56) are related by Fierz transformations. Considering the action of the operators on colour octet ($\frac{1}{\sqrt{3}}T_b$) and singlet states ($\frac{1}{\sqrt{3}}I_3$), and spin-0 ($\frac{1}{\sqrt{2}}I_2$) and spin-1 ($\frac{1}{\sqrt{2}}\sigma_3$) states, we find the relevant Fierz transformations to be

$$\begin{aligned}
d_1 &= 4\pi \frac{1}{6} \left[4b_8 + \frac{4}{3}a_8 + 3b_1 + a_1 \right], \\
d_2 &= 4\pi \frac{1}{6} \left[-\frac{4}{3}b_8 + \frac{4}{3}a_8 - b_1 + a_1 \right], \\
d_3 &= 4\pi \left[-\frac{3}{2}b_8 - \frac{1}{6}a_8 + 3b_1 + a_1 \right], \\
d_4 &= 4\pi \left[\frac{1}{2}b_8 - \frac{1}{6}a_8 - b_1 + a_1 \right].
\end{aligned} \tag{57}$$

Note that the factor of 4π is needed to re-express the contact operators in terms of α_s^2 rather than $\alpha_s g^2$.

From Eq. (56) we see that the energy of colour singlet $\bar{Q}Q$ mesons receives a contributions proportional to d_1 in the spin singlet case and to d_2 for the spin triplet case. The hyperfine splitting is therefore proportional to $(d_1 - d_2)$, cf. subsection VII.VIIA for further discussion. From Eq. (57) we then find

$$d_1 - d_2 = \frac{32\pi}{9} b_8 + \frac{8\pi}{3} b_1, \tag{58}$$

and so the coefficients a_1 and a_8 of the spin-independent operators have cancelled out. In what follows we therefore calculate the coefficients b_8 and b_1 of the spin-dependent operators in Eq. (55).

Since there is no $\sigma \cdot \mathbf{A}$ coupling in NRQCD, it turns out that 1PR diagrams cannot contribute to the spin-dependent non-derivative operators and hence the operator combination which gives rise to the hyperfine splitting can be matched using 1PI diagrams only. In order to complete the matching of all four-fermion operators, including the spin-independent contributions, we need to also calculate the 1PR contributions from inserting the vacuum polarization onto a Coulomb gluon exchange line, since this will generate four-fermion contact operators to all orders in the derivatives. It also turns out that the IR divergences in the spin-independent case are more severe than for the spin-dependent case due in part to these contributions from Coulomb exchange, which also require a careful treatment of lattice artifacts multiplying logarithmic IR divergences. We shall comment further on this observation below and will present the general matching analysis for all non-derivative four-fermion operators in a future paper.

As far as the spin-dependent interactions are concerned, the leading contributions to the four-fermion interactions arise from the 1PI ladder diagrams shown in Figure 5. The box (a) and crossbox (b) diagrams contribute in both continuum QCD and NRQCD, whereas the triangle (c) and diamond (d) diagrams are specific

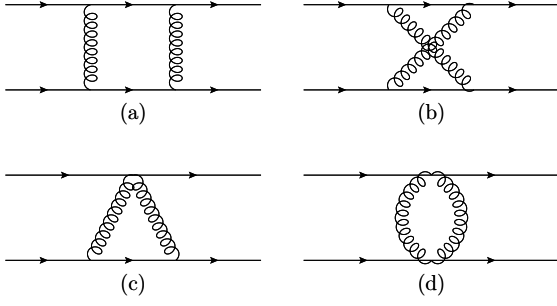


FIG. 5. Ladder Feynman diagrams. Referred to as (a) box, (b) crossbox, (c) triangle, and (d) diamond diagrams. Note that there are two diagrams with the triangle topology.

to NRQCD; again, let us emphasize that these NRQCD-specific diagrams consist not only of lattice artifacts, but also contain continuum contributions from vertices arising from the non-relativistic form of the NRQCD action. Much as in the previous sections, by considering the 1PI diagrams in both continuum QCD and lattice NRQCD, we can then determine the values of the coefficients of the spin-dependent four-fermion operators in the NRQCD action needed to account for radiative improvement corrections.

In addition to the corrections due to $\bar{Q}Q \rightarrow \bar{Q}Q$ scattering calculated above, a further correction to d_1 is required to account for the fact that the NRQCD formalism does not allow for the creation or annihilation of $\bar{Q}Q$ pairs. Figure 6 shows the relevant continuum QCD diagram that is absent in NRQCD. Labelle et al. [8] give the amplitude for this process for QED and it is straightforward to obtain the corresponding QCD result by including the correct colour factors to give [48]

$$d_1^{2-\gamma_{ann}} = -\frac{2}{9} (2 - 2 \ln 2). \quad (59)$$

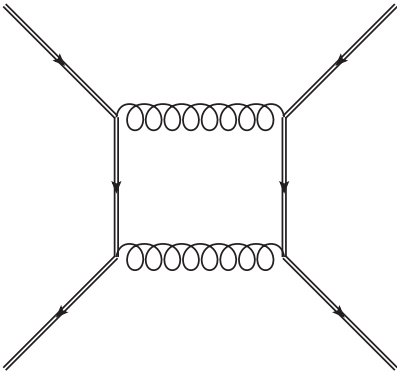


FIG. 6. Two-gluon annihilation diagram

B. Calculation

The absence of a $\bar{Q}Q$ vertex in NRQCD and the fact that quarks and antiquarks have identical masses by the CPT theorem means that the simplest implementation of antiquarks using the HPSRC package is to treat them as just a different species of quark. In fact, we can simply relate QQ -scattering diagrams

$$\begin{aligned} -\Gamma_{\psi^\dagger \psi \psi^\dagger \psi} = & \quad (60) \\ Z_{sym}^{NR,(1)} \frac{\alpha_s g^2}{M^2} (\psi_\alpha^\dagger (iT_a iT_b)_{\alpha\delta} \psi_\delta) (\psi_\beta^\dagger (iT_a iT_b)_{\beta\gamma} \psi_\gamma) \\ & + Z_{asym}^{NR,(1)} \frac{\alpha_s g^2}{M^2} (\psi_\alpha^\dagger (iT_b iT_a)_{\alpha\delta} \psi_\delta) \psi_\beta^\dagger (iT_a iT_b)_{\beta\gamma} \psi_\gamma \\ & + Z_{sym-\sigma}^{NR,(1)} \frac{\alpha_s g^2}{M^2} (\psi_\alpha^\dagger i\sigma (iT_a iT_b)_{\alpha\delta} \psi_\delta) (\psi_\beta^\dagger i\sigma (iT_a iT_b)_{\beta\gamma} \psi_\gamma) \\ & + Z_{asym-\sigma}^{NR,(1)} \frac{\alpha_s g^2}{M^2} (\psi_\alpha^\dagger i\sigma (iT_b iT_a)_{\alpha\delta} \psi_\delta) (\psi_\beta^\dagger i\sigma (iT_a iT_b)_{\beta\gamma} \psi_\gamma), \end{aligned}$$

to the $\bar{Q}Q$ one by changing the representation of one of the quarks appropriately. For NRQED, the antiparticle vertex can be obtained by replacing $e \rightarrow -e$; the NRQCD analogue is taking $(\sigma, T_a) \rightarrow (-\sigma^*, -T_a^T)$ to obtain[49]

$$\begin{aligned} \Gamma_{\chi^\dagger \chi \psi^\dagger \psi} = & \quad (61) \\ -Z_{sym}^{NR,(1)} \frac{\alpha_s g^2}{M^2} (\chi_\alpha^\dagger (T_b T_a)_{\alpha\delta}^T \chi_\delta) (\psi_\beta^\dagger (T_a T_b)_{\beta\gamma} \psi_\gamma) \\ -Z_{asym}^{NR,(1)} \frac{\alpha_s g^2}{M^2} (\chi_\alpha^\dagger (T_a T_b)_{\alpha\delta}^T \chi_\delta) (\psi_\beta^\dagger (T_a T_b)_{\beta\gamma} \psi_\gamma) \\ -Z_{sym-\sigma}^{NR,(1)} \frac{\alpha_s g^2}{M^2} (\chi_\alpha^\dagger \sigma^* (T_b T_a)_{\alpha\delta}^T \chi_\delta) (\psi_\beta^\dagger \sigma (T_a T_b)_{\beta\gamma} \psi_\gamma) \\ -Z_{asym-\sigma}^{NR,(1)} \frac{\alpha_s g^2}{M^2} (\chi_\alpha^\dagger \sigma^* (T_a T_b)_{\alpha\delta}^T \chi_\delta) (\psi_\beta^\dagger \sigma (T_a T_b)_{\beta\gamma} \psi_\gamma), \end{aligned}$$

where the transpose of the individual T_a elements has been pulled outside and the antiquark fields have been relabelled to χ to agree with convention. We have kept all indices explicit to highlight how the creation and annihilation operators are directly replaced.

Dividing out the colour factors and isolating the correct spin structure on both fermion lines passing through the diagram, we can calculate the one-loop coefficients, $Z_{sym}^{NR,(1)}$ etc., directly in the HPSRC code. The factors of i in Eq. (61) come from the convention that we work with anti-hermitian generators when evaluating the colour factors of diagrams. This is convenient since then the commutation relations have real structure constants. Note that by construction the box diagram (a) contributes only to the symmetric colour combination, whereas the crossbox diagram (b) contributes only to the antisymmetric colour combination. The triangle (c) and diamond (d) diagrams contribute to both colour combinations since they contain two-gluon vertices carrying colour factors $\{T_a, T_b\}$.

Although the momentum exchange acts as an IR regulator in these diagrams, we set all three-momenta to zero with the external quarks on-shell and use a gluon mass μ

as the IR regulator using a Stückelberg mass term. This is possible as discussed above, and helps the evaluation by significantly simplifying the pole structure of the integrand: all diagrams have a simple pinch at $k_0 = \pm\mu$, and the calculation can be performed without needing to implement contour shifts in the complex energy plane. As in the case of the BFG vertices, the absence of UV divergences allows us to employ different UV regulators in the QCD and NRQCD calculation.

Radiative improvement is then achieved by adding four-fermion operators to the lattice NRQCD action with coefficients tuned such that one-loop calculations of $QQ \rightarrow QQ$ scattering in NRQCD give the correct continuum QCD result. For example, we add terms such as

$$\Gamma = -Z_{sym}^{(1)} \frac{\alpha_s g^2}{M^2} (\chi_\alpha^\dagger (T_b T_a)^T_{\alpha\delta} \chi_\delta) (\psi_\beta^\dagger (T_a T_b)_{\beta\gamma} \psi_\gamma), \quad (62)$$

where $Z_{sym}^{(1)} = Z_{sym}^{QCD,(1)} - Z_{sym}^{NR,(1)}$ is the difference between the diagrammatic coefficients calculated in continuum QCD and NRQCD, respectively. The radiative improvement can then be implemented with the coefficients

given by

$$a_8 = -\frac{1}{4} \left\{ \left(3 + \frac{5}{3}\right) Z_{sym}^{(1)} + \left(-3 + \frac{5}{3}\right) Z_{asym}^{(1)} \right\}, \quad (63)$$

$$a_1 = -\frac{2}{9} \{ Z_{sym}^{(1)} + Z_{asym}^{(1)} \}, \quad (64)$$

$$b_8 = -\frac{1}{4} \left\{ \left(3 + \frac{5}{3}\right) Z_{sym-\sigma}^{(1)} + \left(-3 + \frac{5}{3}\right) Z_{asym-\sigma}^{(1)} \right\}, \quad (65)$$

$$b_1 = -\frac{2}{9} \{ Z_{sym-\sigma}^{(1)} + Z_{asym-\sigma}^{(1)} \}. \quad (66)$$

The analytical calculation of the continuum QCD diagrams is relatively simple with our choice of IR regulator. The results are

$$Z_{sym}^{QCD,(1)} = -\frac{7}{12\pi} + \frac{1}{4\pi} \log(\mu/M) + \frac{5M}{16\mu} - \frac{M^2}{2\pi\mu^2} + \frac{M^3}{2\mu^3},$$

$$Z_{asym}^{QCD,(1)} = -\frac{3}{4\pi} \log(\mu/M) - \frac{3M}{8\mu} + \frac{M^2}{2\pi\mu^2}, \quad (67)$$

$$Z_{sym-\sigma}^{QCD,(1)} = -\frac{1}{4\pi} + \frac{1}{4\pi} \log(\mu/M) + \frac{M}{6\mu},$$

$$Z_{asym-\sigma}^{QCD,(1)} = -\frac{1}{4\pi} \log(\mu/M). \quad (68)$$

The NRQCD diagrams are computed numerically using the HPsrc package. Since higher order IR divergences dominate numerically, suitable subtraction functions must be chosen to pointwise cancel the divergent integrands:

$$I_{sym}^{sub}(\mu) = -\int \frac{d^4k}{(2\pi)^4} \frac{4\pi M^2(1 + \mathbf{k}^2/4M^2)}{(k^2 + \mu^2)^2(k_0^2 + \mathbf{k}^2/4M^2)} = \tilde{Z}_{sym}^{sub}(\mu) - \frac{1}{\pi} \log(\mu a) - \frac{5M}{16\mu} + \frac{M^2}{2\pi\mu^2} - \frac{M^3}{2\mu^3} \quad (69)$$

$$I_{asym}^{sub}(\mu) = -\int \frac{d^4k}{(2\pi)^4} \frac{4\pi M^2}{(k^2 + \mu^2)^2(ik_0 + \mathbf{k}^2/2M)^2} = \tilde{Z}_{asym}^{sub}(\mu) + \frac{15}{8\pi} \log(\mu a) + \frac{3M}{8\mu} - \frac{M^2}{2\pi\mu^2} \quad (70)$$

$$I_{sym-\sigma}^{sub}(\mu) = -\int \frac{d^4k}{(2\pi)^4} \frac{4\pi}{(k^2 + \mu^2)^2} \left(\frac{\mathbf{k}^2/3}{k_0^2 + \mathbf{k}^2/4M^2} + \frac{1}{2} \right) = \tilde{Z}_{sym-\sigma}^{sub}(\mu) - \frac{1}{4\pi} \log(\mu a) - \frac{M}{6\mu} \quad (71)$$

$$I_{asym-\sigma}^{sub}(\mu) = -\int \frac{d^4k}{(2\pi)^4} \frac{4\pi}{(k^2 + \mu^2)^2} \left(\frac{\mathbf{k}^2/3}{(ik_0 + \mathbf{k}^2/2M)^2} - \frac{1}{2} \right) = \tilde{Z}_{asym-\sigma}^{sub}(\mu) + \frac{1}{4\pi} \log(\mu a) \quad (72)$$

These subtraction functions are continuum-like in that they contain no lattice artifact IR divergences. Evaluating I^{sub} numerically and fitting (with the coefficients of the divergences constrained to agree with the analytical results, and a polynomial in μa added) allows us to determine \tilde{Z}^{sub} . As the integrands are easily evaluated, a large number of points can be sampled. The high-order divergences cause the integrand to become extremely large around $k \sim 0$, which can mean that for small enough k even double-precision variables can overflow, thus returning NaN for the value of the integrand. To avoid this, we add a statement that will set the integrand to zero in a small neighbourhood of the origin. We have to use a sufficient number of VEGAS sampling points in order

to resolve this cut around the origin exactly. In Figures (7)-(8) we plot sample fits of these subtraction functions.

For each colour ordering, the sum of all diagrams is then calculated together with the appropriate subtraction function. In this way all IR divergences except, in some cases, the logarithmic IR divergence are cancelled, regardless of the lattice artifacts, allowing a more constrained fit. For the spin-dependent contribution we calculate

$$Z_{sym-\sigma}^{NR,(1)} + I_{sym-\sigma}^{sub}(\mu) - \tilde{Z}_{sym-\sigma}^{sub}(0) = \tilde{Z}_{sym-\sigma}^{NR,(1)}, \quad (73)$$

$$Z_{asym-\sigma}^{NR,(1)} + I_{asym-\sigma}^{sub}(\mu) - \tilde{Z}_{asym-\sigma}^{sub}(0) = \tilde{Z}_{asym-\sigma}^{NR,(1)}. \quad (74)$$

We evaluate the diagrams for several gluon masses in the range $10^{-3} < \mu^2 < 10^{-2}$, which is chosen such that

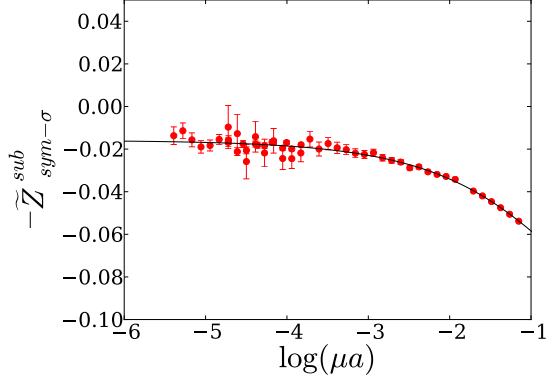


FIG. 7. Sample fit for $\tilde{Z}_{sym-\sigma}^{sub}(\mu)$ for $Ma = 1.95$. We obtain $-0.0159(17) - 0.145(15)\mu a + 0.08(3)(\mu a)^2$ with $\chi^2/d.o.f. = 0.09$.

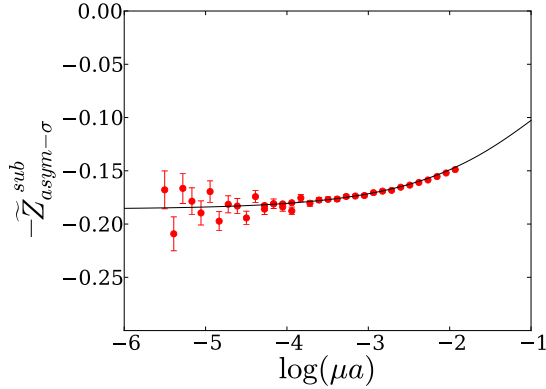


FIG. 8. Sample fit for $\tilde{Z}_{asym-\sigma}^{sub}(\mu)$ for $Ma = 1.95$. We obtain $-0.186(3) + 0.3(1)\mu a - 0.2(3)(\mu a)^2$ with $\chi^2/d.o.f. = 0.08$.

any lattice artifacts (appearing as polynomials in μa) are negligible, yet at the same time large enough such that we do not run foul of any hard-wired numerical tolerances in the HPSRC package.

C. Results

We then have

$$\begin{aligned} Z_{sym-\sigma}^{(1)} &= -\tilde{Z}_{sym-\sigma}^{NR,(1)} - \frac{1}{4\pi} - \frac{1}{4\pi} \log Ma, \\ Z_{asym-\sigma}^{(1)} &= -\tilde{Z}_{asym-\sigma}^{NR,(1)} + \frac{1}{4\pi} \log Ma. \end{aligned}$$

Using these equations, the numerical results for the radiative improvement coefficients b_1 and b_8 for the spin-dependent operators are calculated from Eq. (65) and (66). Results for various NRQCD actions are given in Tables (VI) to (VIII). Note that the coefficients have a

Ma	1.95	2.8	4.0
b_1	0.0037(3)	-0.0201(4)	-0.0490(5)
b_8	0.0893(8)	0.0183(15)	-0.0832(26)

TABLE VI. Renormalization parameters for spin-dependent four-fermion operators, full v^4 NRQCD $n = 2$

Ma	1.9	2.65	3.4
b_1	0.0075(1)	-0.0148(6)	-0.0341(2)
b_8	0.0997(5)	0.0353(1)	-0.0290(8)

TABLE VII. Renormalization parameters for spin-dependent four-fermion operators, full v^4 NRQCD $n = 4$

sizeable dependence on Ma . For the full spin v^6 NRQCD action, this dependence is less pronounced.

As noted at the beginning of this section, we will report on the calculation of the radiative improvement coefficients a_1 and a_8 for the spin-independent operators in Eq. (55) in a future paper.

VII. APPLICATION TO Υ AND η_b SPECTRUM

Having derived the radiative corrections to the $\sigma \cdot B$, Darwin, and spin-dependent four-fermion operators in the NRQCD action, we proceed to analyse the effects of these corrections on the spectrum of mesons containing b-quarks. Depending on whether the operators involved are spin-dependent or not, we can distinguish between changes to the hyperfine splitting and overall shifts of the ground state mass. While obviously no substitute for simulations including the radiatively corrected coefficients in the NRQCD action, estimates for these effects are important because they give a clear indication about the expected magnitude of the corrections to the spectrum of S-wave $b\bar{b}$ states. In what follows the quark mass, M , is identified with the mass, M_b , of the b -quark and defined on the lattice as $a^{-1}(aM_b)$.

A. Hyperfine Splitting

The leading contribution to the hyperfine splitting can be estimated from a perturbative picture involving the exchange of a single gluon between two vertices involving the chromomagnetic operator (cf. Figure 9); this process shifts the energy of a colour-singlet meson state $|M\rangle =$

Ma	1.9	2.65	3.4
b_1	-0.0223(2)	-0.03599(2)	-0.0504(2)
b_8	-0.0280(9)	-0.0624(7)	-0.1071(9)

TABLE VIII. Renormalization parameters for spin-dependent four-fermion operators, full-spin v^6 NRQCD $n = 4$

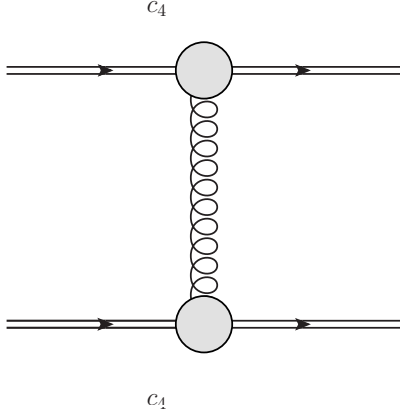


FIG. 9. The tree-level diagram contributing to heavy-heavy meson hyperfine splitting: a spatial gluon is exchanged between two vertices involving the chromomagnetic operator.

$$\frac{1}{\sqrt{3}}|r\bar{r} + b\bar{b} + g\bar{g}\rangle|S\rangle \text{ by}$$

$$\begin{aligned} \Delta E &\approx \frac{c_4^2 g^2}{4M^2} \langle M | (\sigma \times iqT_a)(\sigma^* \times iqT_a^T) | M \rangle / q^2 \\ &= \frac{c_4^2 g^2}{4M^2} \langle S | (\sigma \times iq)(\sigma^* \times iq) | S \rangle \frac{1}{3} \text{Tr}(T_a T_a) / q^2 \\ &= \frac{-2c_4^2 g^2}{9M^2} \langle S | \sigma \cdot \sigma^* | S \rangle. \end{aligned} \quad (75)$$

For $|\eta_b\rangle = \frac{1}{\sqrt{2}}|\uparrow\tilde{\uparrow} + \downarrow\tilde{\downarrow}\rangle$ ($S=0$) and $|\Upsilon\rangle = |\uparrow\tilde{\downarrow}\rangle$ ($S=1$), we have $\langle \eta_b | \sigma \cdot \sigma^* | \eta_b \rangle - \langle \Upsilon | \sigma \cdot \sigma^* | \Upsilon \rangle = 3 - (-1) = 4$, and hence the hyperfine splitting is approximately

$$M_{\eta_b} - M_{\Upsilon} \approx \frac{-8c_4^2 g^2}{9M^2} |\psi(0)|^2, \quad (76)$$

where $\psi(0)$ is the meson wavefunction at the origin, assumed to be the same for the η_b and Υ states. We see that the η_b lies below the Υ , as expected.

Nonperturbative results indicate that the hyperfine splitting in heavy quarkonium is indeed approximately proportional to c_4^2 [5]. Given that the origin of these nonperturbative results can be understood from a tree-level estimate, we can proceed to examine the effect of the four-fermion operators in the same manner. This is straightforward when working in the basis of operators given by Eq. (56), where that we get

$$M_{\eta_b} - M_{\Upsilon} \approx \frac{9(d_1 - d_2)}{2} \alpha_s^2 \frac{4}{3M^2} |\psi(0)|^2 \quad (77)$$

for the four-fermion contribution to the hyperfine splitting, which can be re-expressed in term of the coefficients a_i, b_i using Eq. (57).

The one-loop correction to the hyperfine splitting is then estimated to be the tree-level value multiplied by the one-loop correction factor

$$1 + \alpha_V(q^*) \left(2c_4^{(1)} - \frac{9}{8} \left(\frac{16}{3}b_8 + 4b_1 \right) + \frac{3}{8\pi} (2 - 2\ln 2) \right). \quad (78)$$

In Table IX we give our estimates for the corrections that need to be applied to the hyperfine splitting as measured in full v^4 NRQCD $n = 2$ without perturbative improvements. Applying our estimated correction *post hoc* to the data presented by the HPQCD collaboration in [1], we find that the corrections to the chromomagnetic operator and the inclusion of the spin-dependent four-fermion terms work to increase the hyperfine splitting, pushing it closer to the experimental value of 69.3(2.8)MeV [10]. We note that the corrections from the four fermion operators further reduce the lattice spacing dependence, as can be seen from the results plotted in Figure 10. It is important to note that for the $O(v^4)$ NRQCD action the errors on the corrected results include an estimate of the

effect of the omitted $O(v^6)$ term shown in Eq. (5), and that these errors are preliminary in the sense that future simulations will include these terms explicitly, using the results of this paper, and removing the need for a *post hoc* correction.

In Table X and Figure 11 we present the corrections to the full v^4 NRQCD $n = 4$ hyperfine splitting as measured in [2], where the perturbatively corrected coefficient c_4 has been included in the simulation, and only the four-fermion operator corrections need to be applied by hand. As in $n = 2$ case, the corrected chromomagnetic operator acts to increase the hyperfine splitting, and the four-fermion corrections reduce the lattice spacing dependence (which however is less severe from the

M	β	α_V	c_4 correction	box correction	total	old hfs	new hfs
1.95	7.09	0.216	+31.4(3)%	-10.4(1)%	+21.0(3)%	56(2)	68(3)(5)(6)
2.8	6.76	0.249	+39.8(3)%	+1.3(2)%	+41.1(4)%	50(2)	71(3)(6)(5)
4.0	6.458	0.293	+49.3(3)%	+23.2(3)%	+72.5(4)%	41(2)	71(3)(7)(4)

TABLE IX. Estimates of the corrections to the bottomonium hyperfine splitting results of [1] arising from the radiative improvement of the $n = 2$ full v^4 NRQCD action. The errors given in the last column are statistical, $O(\alpha_s^2)$, and relativistic corrections, in that order.

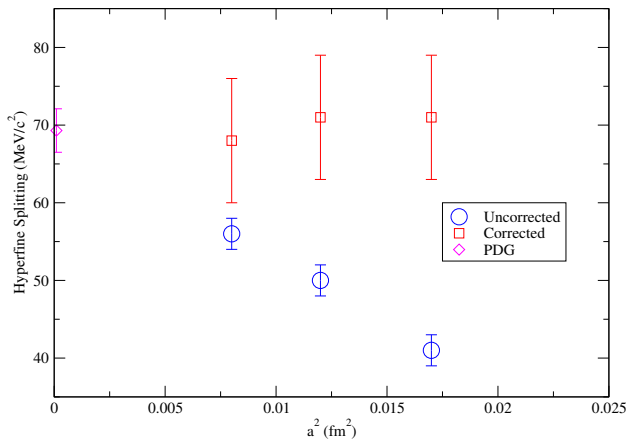


FIG. 10. Comparison of the corrected and uncorrected bottomonium hyperfine splitting results for $n = 2$ full v^2 NRQCD [1]. Note that for the corrected results the total error including estimates of the effects of $O(\alpha_s^2)$ contributions and $O(v^6)$ terms omitted in the simulation is displayed, whereas the uncorrected results are shown with statistical errors only, since their $O(\alpha_s)$ errors would be too large to show on this scale. The PDG data point is taken from [10].

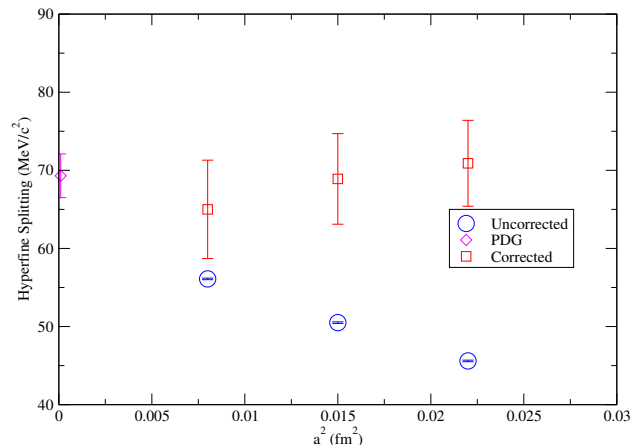


FIG. 11. Comparison of the corrected and uncorrected bottomonium hyperfine splitting results for $n = 4$ full v^4 NRQCD [2]. Note that for the corrected results the total error including estimates of the effects of $O(\alpha_s^2)$ contributions and $O(v^6)$ terms omitted in the simulation is displayed, whereas the uncorrected results are shown with statistical errors only, since their $O(\alpha_s)$ errors would be too large to show on this scale. The PDG data point is taken from [10].

Ma	$\alpha_V(q^*)$	hfs (MeV)		Correction 4-fermion	hfs (MeV) corrected
		$c_4 = 1$	improved c_4		
1.9	0.225	56.1(1)	72.1(1)	-12.6(1)%	65.0(1)(2.8)(5.6)
2.65	0.253	50.5(1)	69.8(1)	-1.8(1)%	68.9(1)(3.2)(5.0)
3.4	0.275	45.6(1)	65.6(1)	+11.0(1)%	70.6(1)(3.4)(4.6)

TABLE X. The corrections to the bottomonium hyperfine splitting arising from the radiative improvement of the $n = 4$ full v^4 NRQCD action, as found in [2]. Only the four-fermion contributions are *post hoc* estimates. The errors given in the last column the errors are statistical, $O(\alpha_s^2)$, and relativistic corrections, in that order.

outset when comparing to the $n = 2$ case).

Finally, in Table XI we estimate the relative corrections from the corrected coefficients to full $n = 4$ NRQCD results when including the spin-dependent v^6 terms in the action. While the corrections arising from the improvement of the chromomagnetic term are similar to the case of full $n = 4$ v^4 NRQCD, the corrections coming from the four-fermion operators are significantly larger. While one might naively expect that the effect of radiative corrections ought to decrease as higher-order terms are added

M	α_V	c_4 correction	box correction
1.9	0.225	+37(4)%	+7.7(1)%
2.65	0.253	+40(4)%	+15.4(1)%
3.4	0.275	+26(4)%	+25.9(1)%

TABLE XI. Corrections to the bottomonium hyperfine splitting arising from the radiative improvement of the $n =$ full NRQCD action including spin-dependent terms at order v^6 .

to the action, it has been shown in [5] that the inclusion of $O(v^6)$ terms (albeit with a different gauge action) leads to a decrease of the (tree-level) hyperfine splitting. It appears that the larger corrections from the four-fermion operators would compensate for this effect.

The radiative corrections to the chromomagnetic operator (but not the four-fermion operators) will also affect the hyperfine splitting in heavy-light mesons through the leading perturbative contribution shown in Figure 12, giving a hyperfine splitting approximately proportional to c_4 . Besides the absence of the four-fermion terms, heavy-light systems also benefit from much smaller v^6 corrections, which makes them a particularly suitable

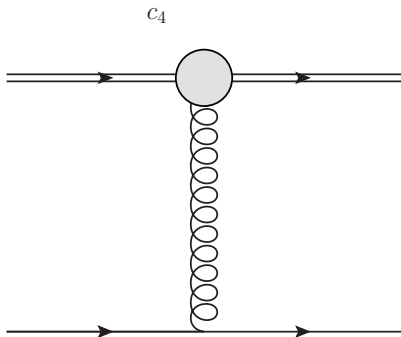


FIG. 12. The tree-level diagram contributing to the hyperfine splitting in heavy-light mesons: a spatial gluon is exchanged between two vertices, the heavy-quark one of which involves the chromomagnetic operator.

test case for assessing the efficiency of including the radiative corrections. In [3], the NRQCD action with radiatively improved coefficients was used for the first time for the heavy-light B -meson system. The results for the hyperfine splittings for the B and B_s mesons show little a^2 dependence, and even for coarse lattices are in very good agreement with experimental data; this gives a strong check on the correctness and usefulness of the radiative corrections and lends credibility to the prediction (rather than postdiction) of $M_{B_c^*} - M_{B_c} = 54(3)$ MeV [3] incorporating the effects of radiatively improving c_4 .

$$\Delta E \approx \frac{-g^2}{3M^2} \left(1 + \alpha_s(c_2^{(1)} - 12b_8 - 4a_8 - 9b_1 - 3a_1 + \frac{1}{\pi}(2 - 2 \ln 2)) \right) |\psi(0)|^2, \quad (82)$$

giving an effective value of $c_2^{eff} = 1 + \alpha_s(c_2^{(1)} - 12b_8 - 4a_8 - 9b_1 - 3a_1 + \frac{1}{\pi}(2 - 2 \ln 2))$. From this expression it is clear that we cannot consider the correction due to the Darwin operator in isolation, but must include the effects of the spin-independent four-fermion operators which we have not computed in this paper and whose calculation will be presented in a forthcoming paper.

VIII. CONCLUSIONS

In this paper, we have applied the BF method to lattice NRQCD and have computed the one-loop radiative correction to the coefficient, c_4 , of the $\boldsymbol{\sigma} \cdot \mathbf{B}$ and the one-loop radiative contribution to the coefficients, d_1 and d_2 of the four-fermion contact operators that affect the hyperfine structure of heavy quark mesons. The gauge independence of our calculation was explicitly checked by carrying out both relativistic and non-relativistic calculations in the lattice theory. This is possible because in BFG all calculations are UV finite.

B. Mass shift

The leading spin-independent perturbative correction to the energy of a meson state is given by the single-gluon exchange involving the Darwin term at one of the vertices, as shown in Figure 13. This gives the energy shift from the corrected c_2 coefficient as

$$\Delta E \approx \frac{2c_2 g^2}{8M^2} \langle M | (q^2 T_a)(T_a^T) | M \rangle / q^2 \quad (79)$$

$$= \frac{-c_2 g^2}{3M^2} |\psi(0)|^2. \quad (80)$$

The corresponding contribution from the four-fermion operators gives

$$\Delta E \approx \frac{9d_1}{2} \alpha_s^2 \frac{4}{3M^2} |\psi(0)|^2. \quad (81)$$

While the hyperfine splitting between the η_b and Υ states will lead to higher-order corrections to their wavefunctions at the origin, to leading order these can be taken to be identical, here denoted $\psi(0)$, giving the same shift in mass for both states.

Again, there is no real substitute for including the four-fermion operators in numerical simulations; however, we can attempt to estimate the size of their overall effect by determining an effective value for c_2 using the tree-level approximations given above.

Combining Eqs. (80) and (81), we find

Our results are summarized in Tables IX, X, and XI, and in Eqs. (32), (78) and (82). In particular, in eqn. (32) there is a negative correction to c_4 due to the effect of the continuum logarithmic IR divergence. However, it turns out that the constant terms more than cancel this effect and the correction to c_4 is positive.

Whilst no substitute for including these corrections in a simulation, our estimate for the correction to the $\Upsilon - \eta_b$ hyperfine splitting measured by Gray et al. [1], as shown in table IX, indicates that the effect of the corrections is to reduce the lattice spacing dependence to within the remaining errors. The resulting estimate for the hyperfine splitting of 68(3)(5)(3) MeV is then in good agreement with the experimental value of 69.3(2.8) MeV [10]. Subsequent simulations [2, 3] have confirmed these expectations. It will be interesting to see how the inclusion of our radiative corrections in simulations utilizing the $O(v^6)$ NRQCD action will compare with the results of [5], where a reduced hyperfine splitting was found when using the tree-level $O(v^6)$ NRQCD action; from our results, we expect that the inclusion of the four-fermion

operators will compensate for this reduction.

The elimination of $O(\alpha_s a^2)$ errors, the much reduced dependence of observables on a^2 and the agreement with experiment gives us confidence that the improvement strategy for constructing the NRQCD effective action is robust.

ACKNOWLEDGMENTS

We thank Christine Davies, Alan Gray, Andrew Lee, Peter Lepage, John Gracey and Matthew Wingate for useful discussions. We thank the DEISA Consortium (<http://www.deisa.eu>), co-funded through the EU FP6 project RI-031513 and the FP7 project RI-222919, for support within the DEISA Extreme Computing Initiative. This work was supported by STFC under grants ST/G000581/1 and ST/H008861/1. The calculations for this work were, in part, performed on the University of Cambridge HPCs as a component of the DiRAC facility jointly funded by STFC and the Large Facilities Cap-

ital Fund of BIS. The University of Edinburgh is supported in part by the Scottish Universities Physics Alliance (SUPA).

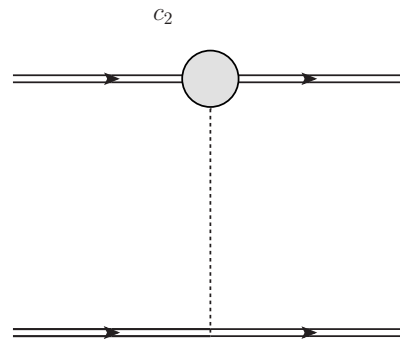


FIG. 13. The tree-level diagram contributing to the ground state mass shift: a temporal gluon is exchanged between two vertices, one of which involves the Darwin operator.

-
- [1] HPQCD and UKQCD Collaborations, A. Gray *et al.*, Phys. Rev. D **72**, 094507 (2005).
 - [2] HPQCD Collaboration, R. Dowdall *et al.*, Phys.Rev. **D85**, 054509 (2012), [1110.6887].
 - [3] R. Dowdall, C. Davies, T. Hammant and R. Horgan, Phys.Rev. **D86**, 094510 (2012), [1207.5149].
 - [4] G. P. Lepage, L. Magnea, C. Nakhleh, U. Magnea and K. Hornbostel, Phys. Rev. D **46**, 4052 (1992).
 - [5] S. Meinel, Phys.Rev. **D82**, 114502 (2010), [1007.3966].
 - [6] T. Kinoshita and M. Nio, Phys.Rev. D **53**, 4909 (1996), [hep-ph/9512327].
 - [7] M. Nio and T. Kinoshita, Phys. Rev. D **55**, 7267 (1997).
 - [8] P. Labelle, S. M. Zebarjad and C. P. Burgess, Phys. Rev. D **56**, 8053 (1997), [hep-ph/9706449].
 - [9] T. C. Hammant, A. G. Hart, G. M. von Hippel, R. R. Horgan and C. J. Monahan, Phys. Rev. Lett. **107**, 112002 (2011).
 - [10] K. Nakamura *et al.*, J. Phys. G **37**, 075021 (2010).
 - [11] B. S. DeWitt, Phys.Rev. **162**, 1195 (1967).
 - [12] B. S. DeWitt, Phys.Rev. **162**, 1239 (1967).
 - [13] H. Kluberg-Stern and J. Zuber, Phys.Rev. **D12**, 482 (1975).
 - [14] L. Abbott, M. Grisaru and R. Schaefer, Nucl.Phys. **B229**, 372 (1983).
 - [15] G. Vilkovisky, in: *Quantum theory of gravity, essays in honor of 60th Birthday of Bryce S. DeWitt* (A. Hilger, 1984).
 - [16] A. Rebhan, Nuclear Physics B **288**, 832 (1987).
 - [17] G. 't Hooft, Nucl.Phys. **B153**, 141 (1979).
 - [18] P. Weisz and R. Wohlert, Nucl. Phys. B **236**, 397 (1984).
 - [19] M. Lüscher and P. Weisz, Nuclear Physics B **266**, 309 (1986).
 - [20] HPQCD Collaboration, A. Hart, G. von Hippel and R. Horgan, Phys.Rev. **D79**, 074008 (2009), [0812.0503].
 - [21] G. Curci and R. Ferrari, Nuovo Cim. **A32**, 151 (1976).
 - [22] G. Curci and R. Ferrari, Nuovo Cim. **A35**, 1 (1976).
 - [23] G. Curci and E. d'Emilio, Phys.Lett. **B83**, 199 (1979).
 - [24] I. Ojima, Z.Phys. **C13**, 173 (1982).
 - [25] A. Blasi and N. Maggiore, Mod.Phys.Lett. **A11**, 1665 (1996), [hep-th/9511068].
 - [26] J. Gracey, Phys.Lett. **B525**, 89 (2002), [hep-th/0112014].
 - [27] J. Gracey, Phys.Lett. **B552**, 101 (2003), [hep-th/0211144].
 - [28] R. Browne and J. Gracey, Phys.Lett. **B540**, 68 (2002), [hep-th/0206111].
 - [29] K.-I. Kondo, K. Suzuki, H. Fukamachi, S. Nishino and T. Shinohara, Phys.Rev. **87**, 025017 (2013), [1209.3994].
 - [30] L. von Smekal, M. Ghiotti and A. G. Williams, Phys.Rev. **D78**, 085016 (2008), [0807.0480].
 - [31] M. E. Peskin and D. V. Schroeder, *An Introduction to quantum field theory* (Westview Press, Boulder, 1995).
 - [32] S. Kautsky, Master's Thesis, Simon Fraser University 2006, unpublished.
 - [33] C. Davies and B. Thacker, Phys.Rev. **D45**, 915 (1992).
 - [34] B. A. Thacker and G. P. Lepage, Phys. Rev. D **43**, 196 (1991).
 - [35] S. Groote and J. Shigemitsu, Phys.Rev. **D62**, 014508 (2000), [hep-lat/0001021].
 - [36] BABAR Collaboration, B. Aubert *et al.*, Phys. Rev. Lett. **101**, 071801 (2008).
 - [37] A. Hart, G. von Hippel, R. Horgan and E. Mller, Computer Physics Communications **180**, 2698 (2009).
 - [38] L. L. Foldy and S. A. Wouthuysen, Phys. Rev. **78**, 29 (1950).
 - [39] S. Tani, Progress of Theoretical Physics **6**, 267 (1951).
 - [40] G. von Hippel, Comp. Phys. Comm. **174**, 569 (2006).
 - [41] G. von Hippel, Comp. Phys. Comm. **181**, 705 (2010).
 - [42] L. Khomskii, *Perturbation Theory for Quarks and Currents in Moving NRQCD on a Lattice*, PhD thesis, University of Cambridge, 2008.
 - [43] R. Horgan *et al.*, Phys. Rev. D **80**, 074505 (2009).

- [44] Wolfram Research, Inc., Mathematica[®] version 8.0.1, 2011.
- [45] E. Müller, *Heavy-to-light Decays on the Lattice*, PhD thesis, University of Edinburgh, 2009.
- [46] M. A. Nobes, H. D. Trottier, G. P. Lepage and Q. Mason, Nucl.Phys.Proc.Suppl. **106**, 838 (2002), [hep-lat/0110051].
- [47] A. A. Penin, arXiv:0905.4296.
- [48] A. Pineda and J. Soto, Phys.Rev. **D58**, 114011 (1998), [hep-ph/9802365].
- [49] We have used the convention that the anti-quark fields are in the $\bar{\mathbf{2}}$ representation, whereas some other authors put them in the $\mathbf{2}$ representation. The two conventions can be related using the charge conjugation matrix $C = i\sigma_2$.